

Stimuli-responsive and self-healing supramolecular Zn (II)-guanosine metal-organic gel for Schottky barrier diode application

Surbhi Singh,^a Atul Kumar Sharma,^b Hrushikesh M. Gade,^c Vidhi Agarwal,^d Nasani Rajendar,^e Nisha Verma,^a and Bhagwati Sharma^{*a}

^a*Materials Research Centre, Malaviya National Institute of Technology Jaipur, Malviya Nagar, Jaipur 302017, India.*

Email: bhagwati.mrc@mnit.ac.in

^b*Department of Electronics and Communication Engineering, Malaviya National Institute of Technology Jaipur, Malviya Nagar, Jaipur 302017, India.*

^c*Department of Chemical Engineering, Malaviya National Institute of Technology Jaipur, Malviya Nagar, Jaipur 302017, India.*

^d*Department of Chemistry, Indian Institute of Technology Indore, Simrol, Khandwa Road, Indore 453552, India.*

^e*School of Chemistry, University of Hyderabad, Gachibowli, Hyderabad-500046, India.*

Molecular dynamics simulations:

MD simulations were conducted for a model of guanosine, Zinc acetate and NaOH (gel). The simulation system comprised of proportional number of molecules (10 molecules of guanosine/10 molecules of Zinc Acetate/20 molecules of NaOH/~11000 molecules of water) equivalent to experimental composition (0.1 mmol Guanosine/ 0.1 mmol Zinc Acetate/0.2 mmol NaOH/0.111 mol Water). The system was prepared using the Packmol software¹ and then solvated using tip4p water model. The molecules were parameterized using OPLS-AA force-field.² Simulations were conducted using Gromacs simulation Engine.³ The cut-off distance for van der Waals (vdW) and coulombic interactions was set at 10 Å. The long-range coulombic interactions are evaluated using the particle mesh Ewald method. Each of the simulation system is initially equilibrated for 1 ns using the NPT ensemble with exponential relaxation of Berendsen thermostat and barostat to reach the desired conditions of 300 K and 1 bar followed by 50 ns production run in NPT ensemble with oscillatory relaxation with Nose-Hoover thermostat and Parinello-Rahman Barostat. Molecular motion equations are integrated using the leap-frog algorithm with 2-femtosecond time steps. Using the LINCS algorithm, molecular bonds are restricted. The molecular coordinates are stored every 1 picosecond for post-simulation analysis.

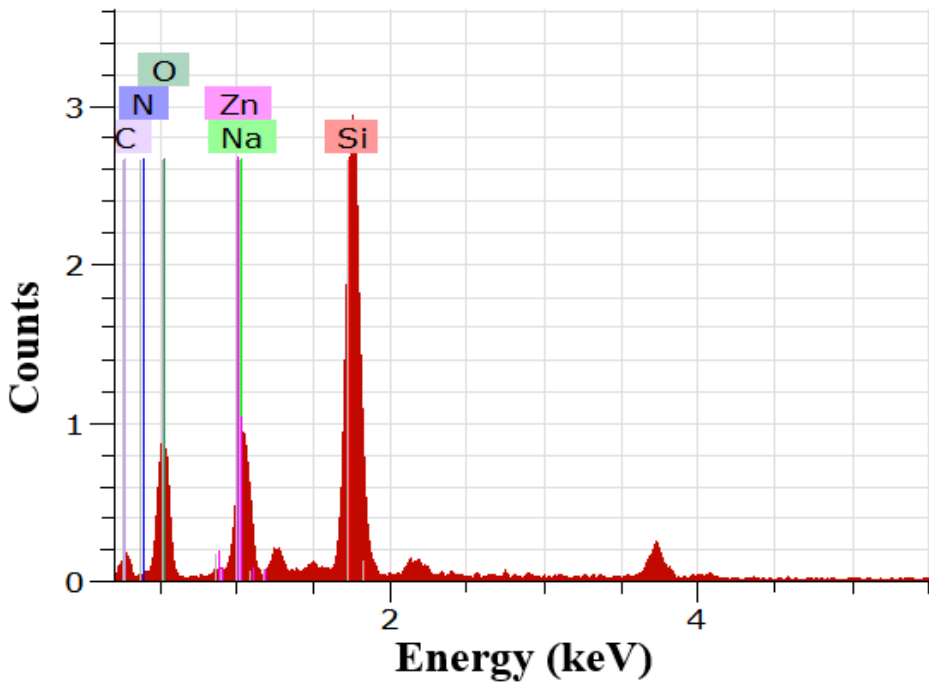


Figure.S1 EDX Spectrum showing the presence of C, N, O, Na, and Zn in Zn-guanosine metallogel.

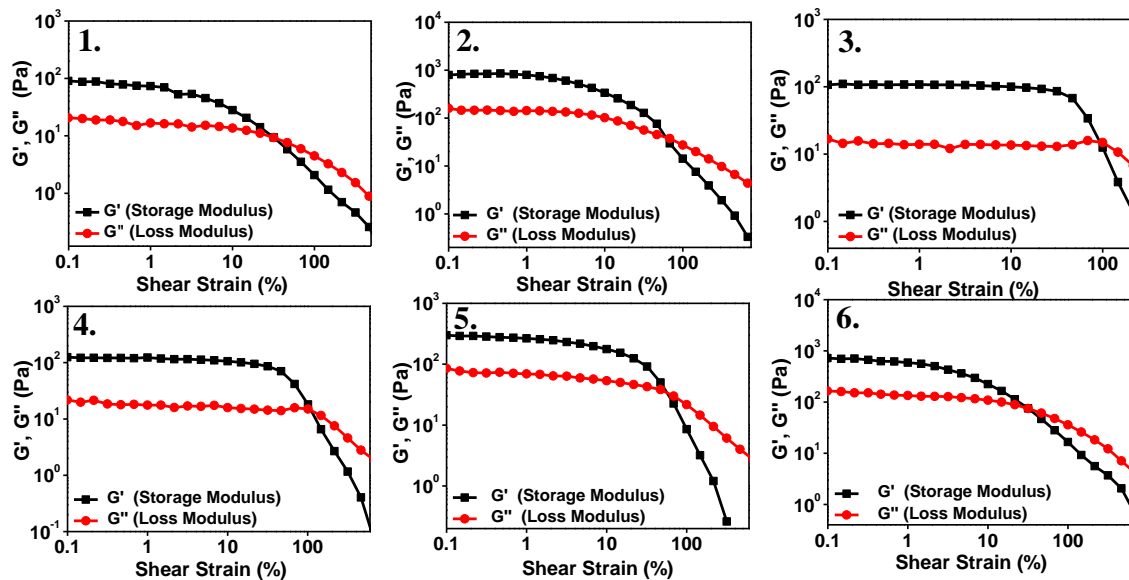


Figure.S2 Rheological investigations of the Zn-guanosine metallogel, dynamic strain sweep rheological investigation at varying G:Zn molar concentrations (1) 0.025M : 0.1M (2) 0.05M : 0.1M (3) 0.075M : 0.1M (4) 0.1M : 0.1M (5) 0.1M : 0.05M (6) 0.1M : 0.025M.

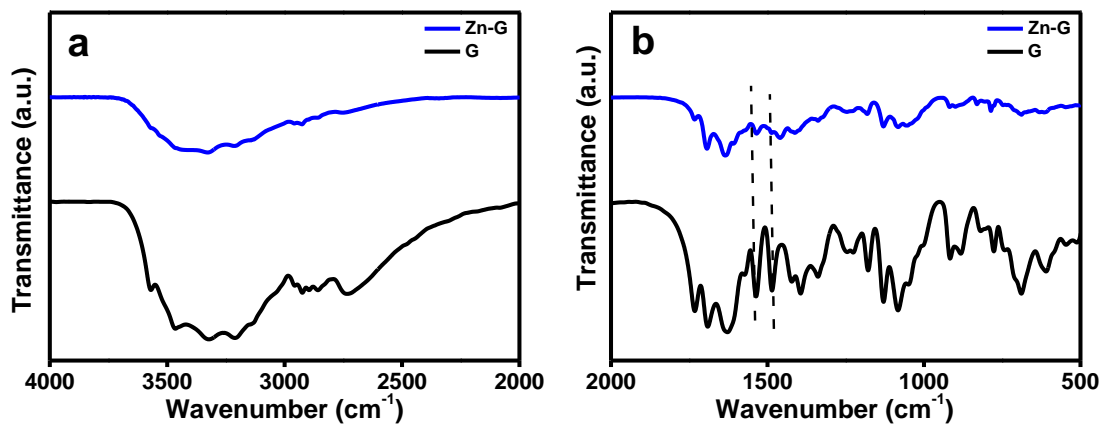


Figure.S3 FTIR spectrum of the pure guanosine and freeze-dried Zn-guanosine xerogel.

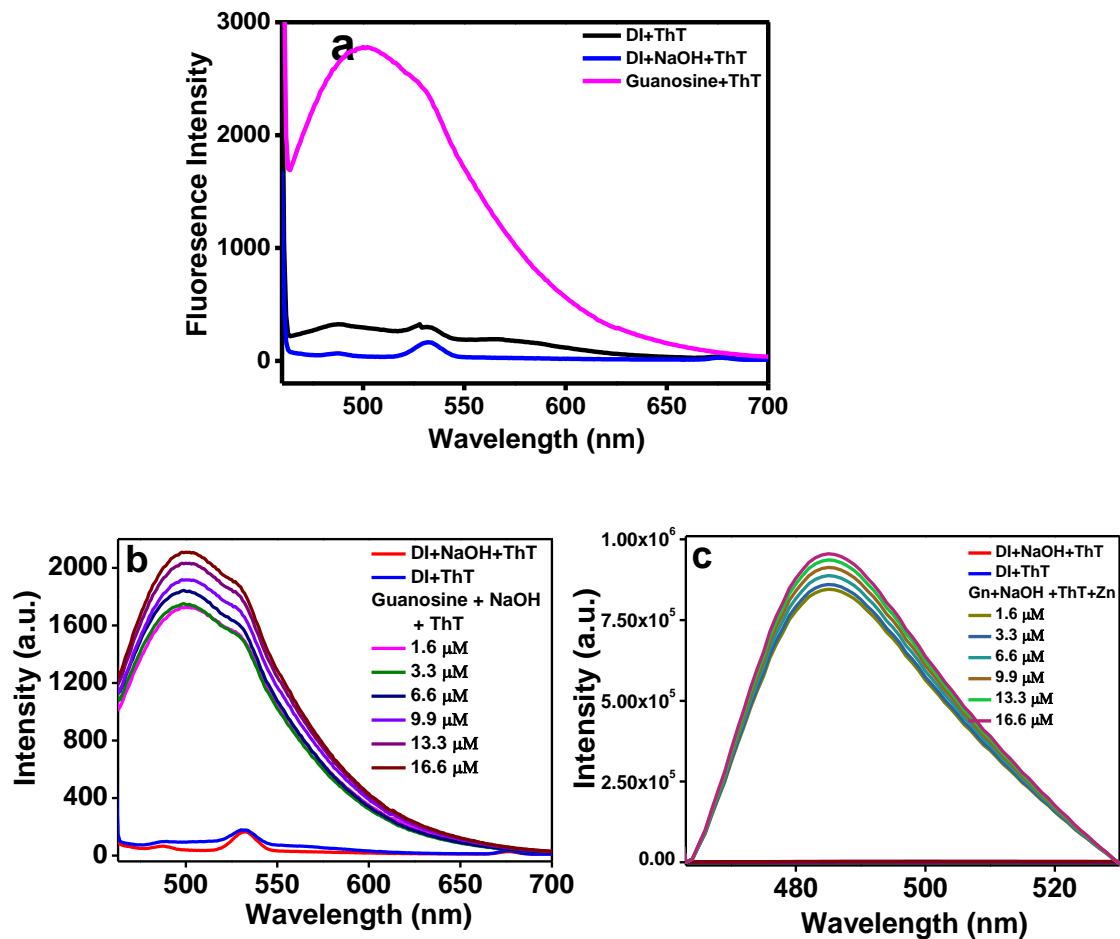


Figure S4. (a) Fluorescence emission spectrum of ThT in pure water (black line), 0.2 M NaOH (blue line), and guanosine in NaOH (pink line), The FL spectra of ThT at varying concentration from 1.7 to 17 μM for (b) guanosine in NaOH and (c) guanosine in NaOH followed by addition of zinc ions.

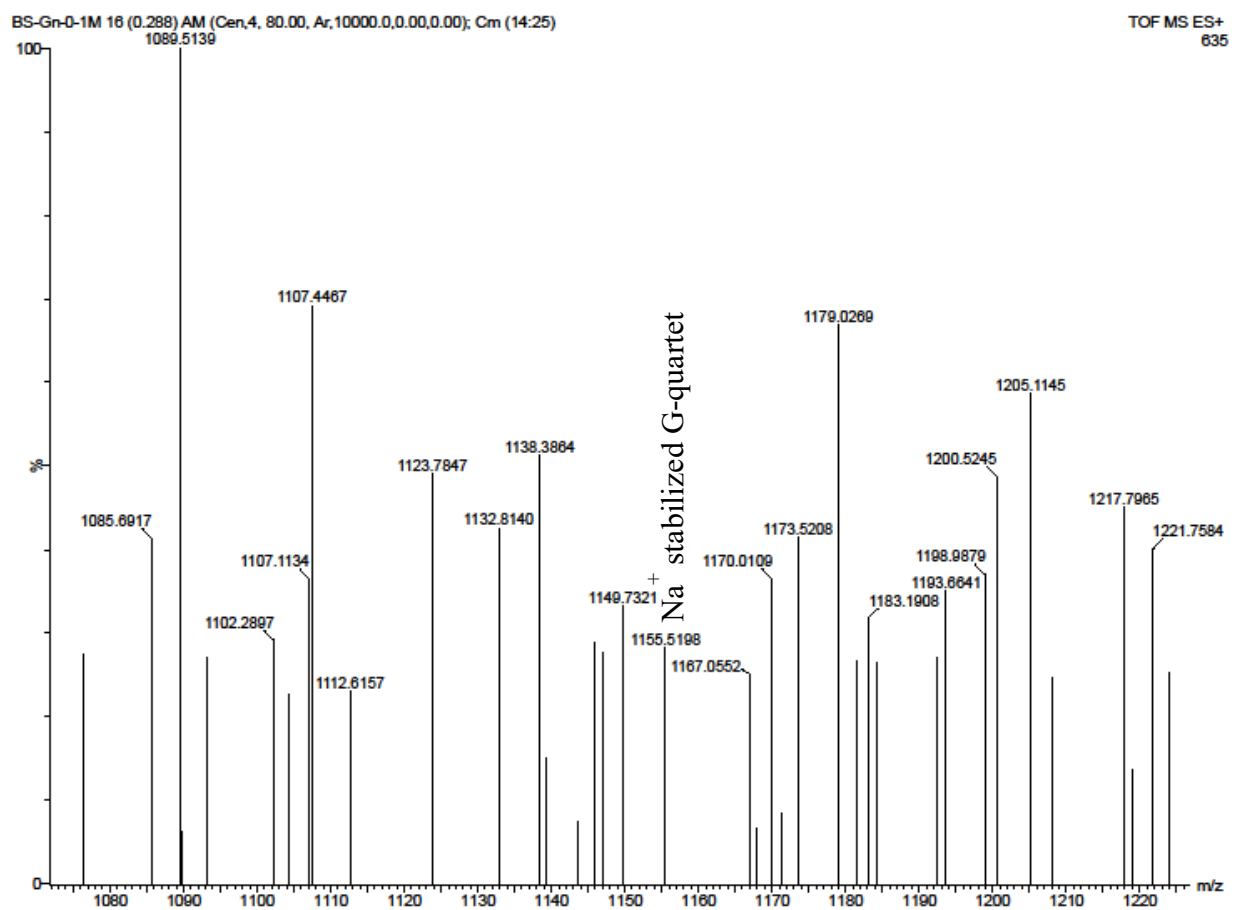


Figure S5. ESI- MS spectrum of guanosine in the presence of NaOH.

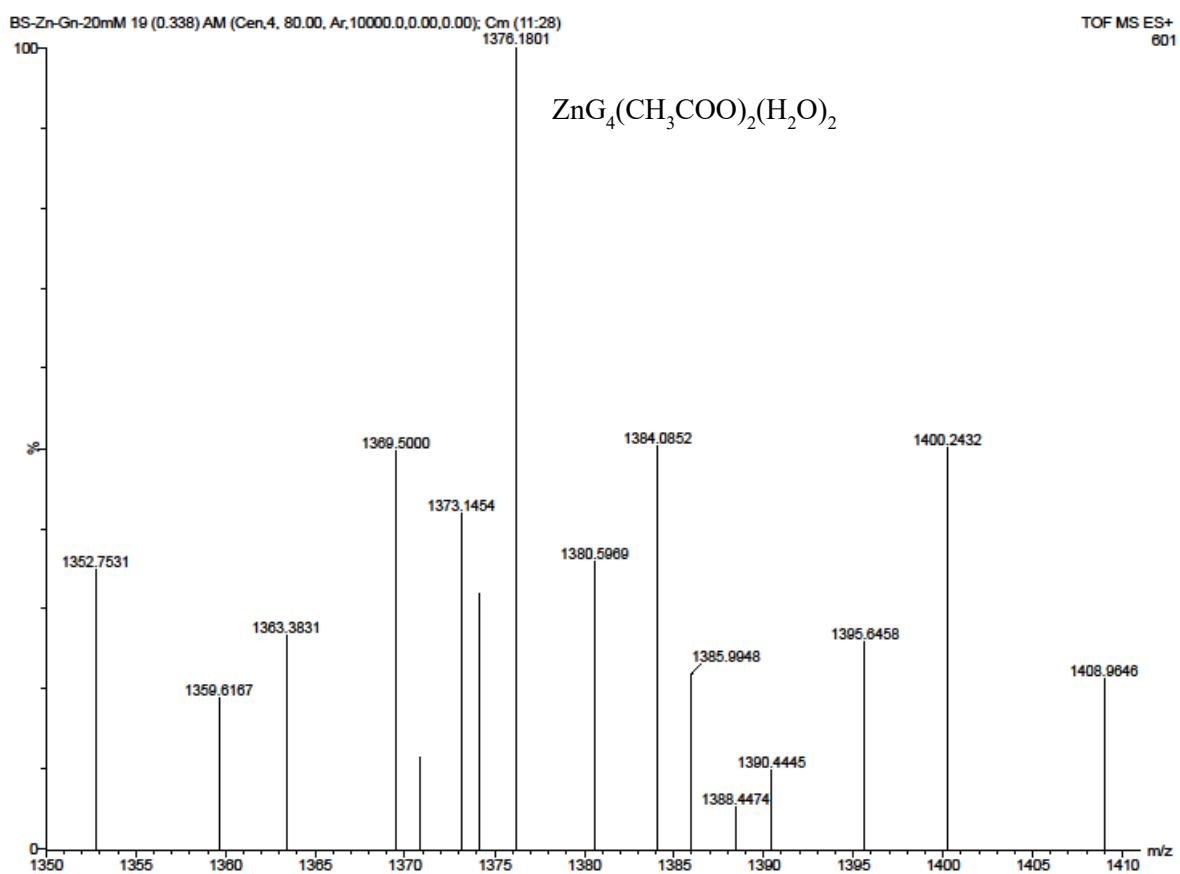


Figure S6. ESI- MS spectrum of a 1:1 mixture of guanosine and Zn-acetate (both 20 mM).

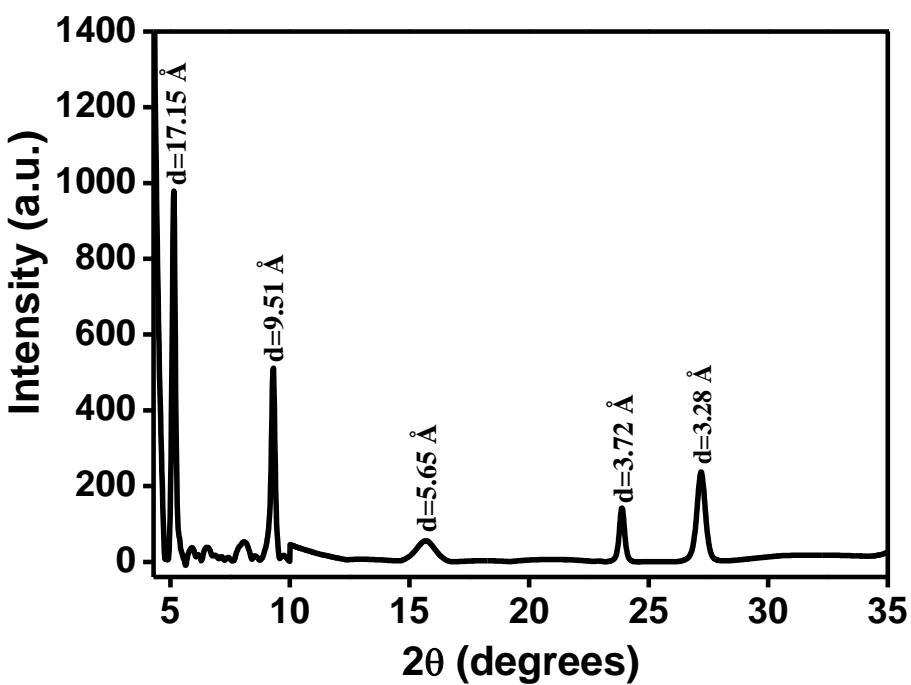


Figure S7. PXRD pattern of the freeze-dried Zn-Guanosine xerogel.

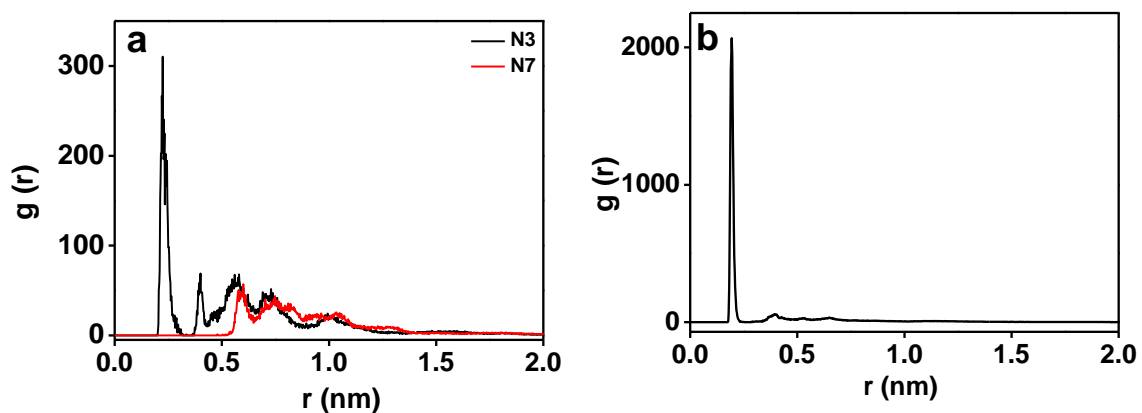


Figure S8. (a) Radial distribution function between N(3)/N(7) and Zn^{2+} ions and (b) the radial distribution function between oxygen atom of acetate and Zn^{2+} ions.

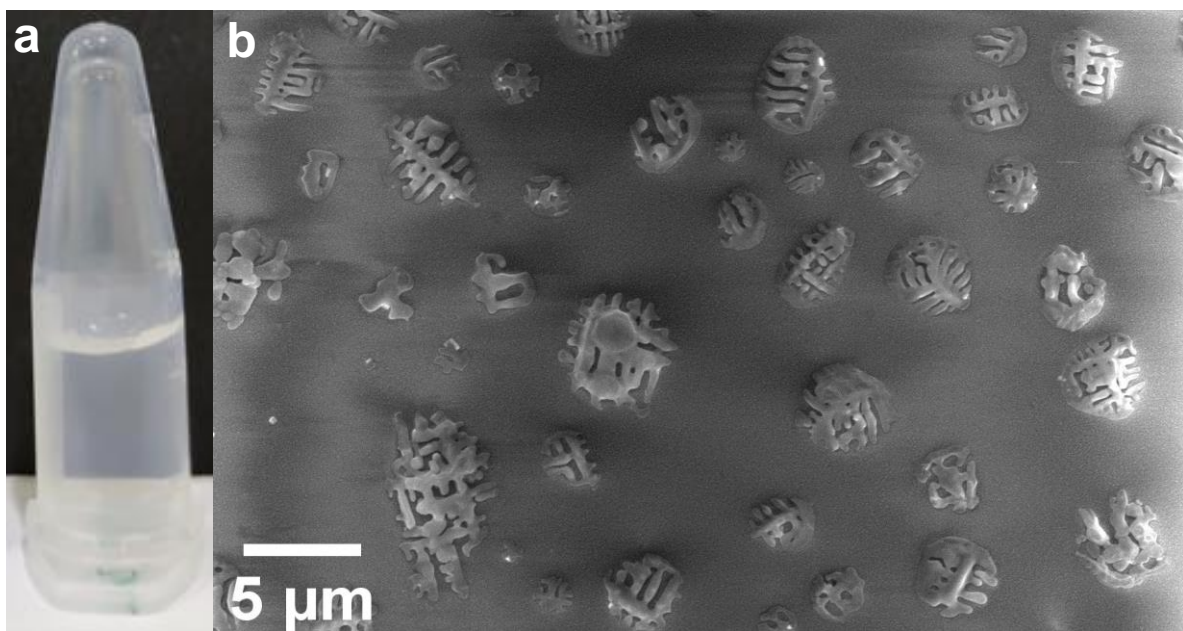


Figure.S9 (a) Digital image of a 1:1 mixture of guanosine (dissolved in 1M HCl) and Zn-acetate, showing the formation of a clear solution and (b) SEM image of the Zn-guanosine mixture under acidic conditions.

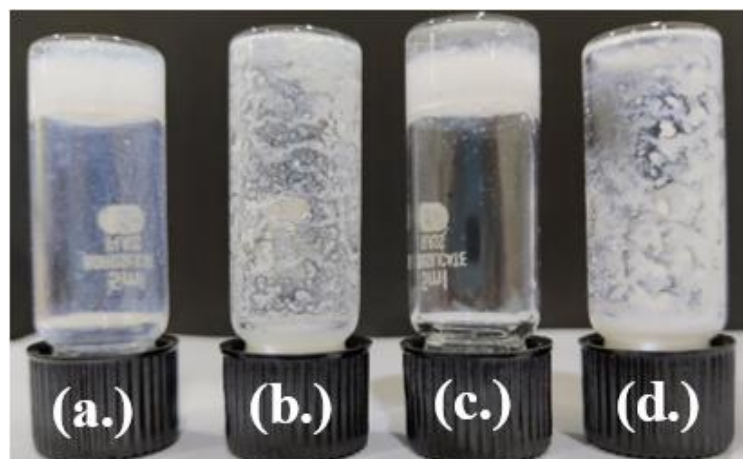


Figure.S10 Digital images of Zn-Guanosine mixtures in different solvents (a) methanol-water (gel) (b) methanol-methanol (precipitate) (c) ethanol-water (gel) and (d) ethanol-ethanol (precipitate) respectively.

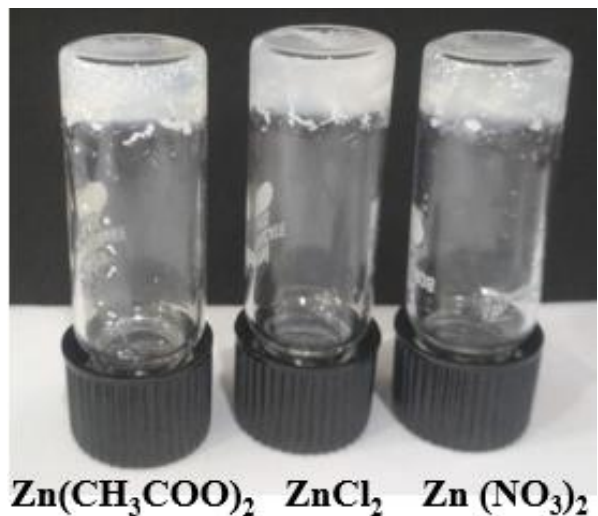


Figure S11. Digital images showing the formation of stable gels upon changing of metal counterions viz. $\text{Zn}(\text{CH}_3\text{COO})_2$, ZnCl_2 and $\text{Zn}(\text{NO}_3)_2$ respectively.

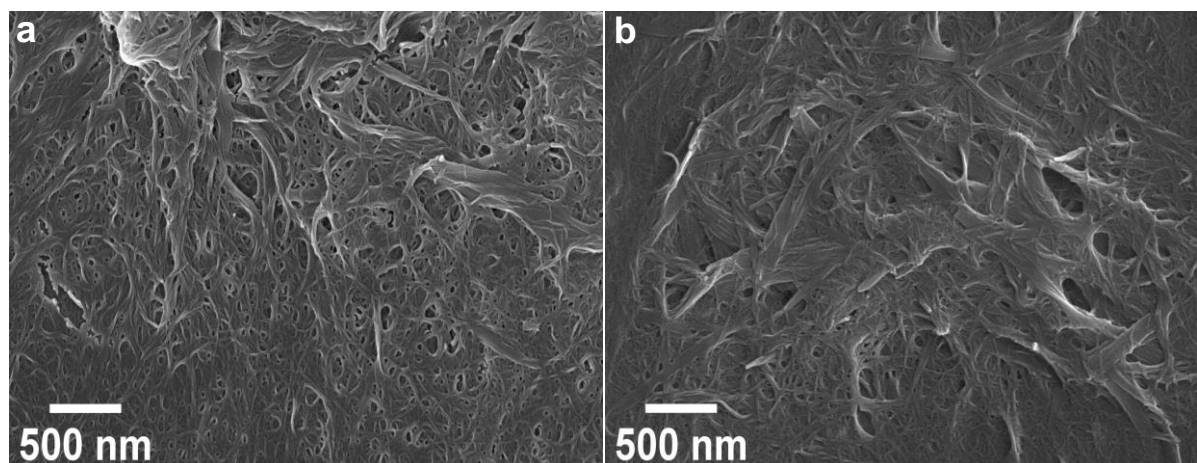


Figure S12. FESEM images showing the formation of fibers upon changing of metal counterions (a) Zinc Nitrate, and (b) Zinc Chloride.

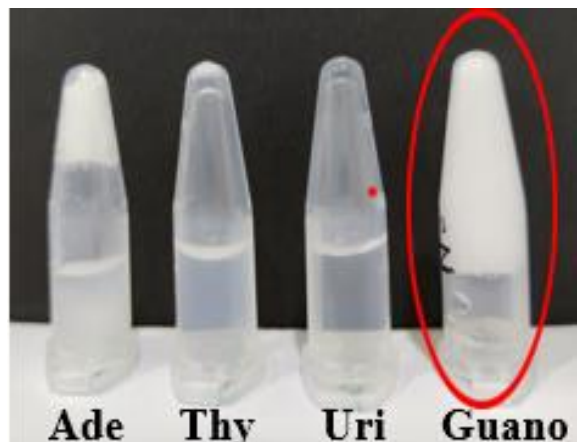


Figure S13. Digital images showing the formation of precipitates or turbid sol upon the interaction of adenine, thymidine, and uridine with Zn^{2+} ions.

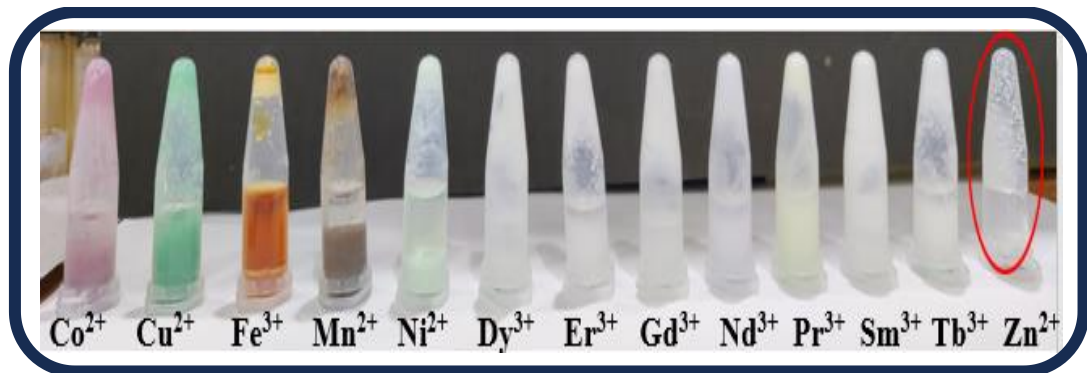


Figure S14. Digital images showing the specificity of Zn^{2+} ions towards the formation of hydrogel upon interaction with guanosine.

Table S1. Interaction of guanosine with Zn^{2+} ions with varying molar ratios (With a variation in the molar concentration of both the reactants).

S.No	Molar Concentration (M)		Result	% Strain at which G'' dominates G' in amplitude sweep experiment
	Guanosine (M)	Zinc Acetate (M)		
1.	0.025	0.1	Very Weak Gel	30.97
2.	0.05	0.1	Weak Gel	57.53
3.	0.075	0.1	Gel	94.5
4.	0.1	0.1	Gel	110
5.	0.1	0.05	Weak Gel	56.76
6.	0.1	0.025	Very weak Gel	30.87

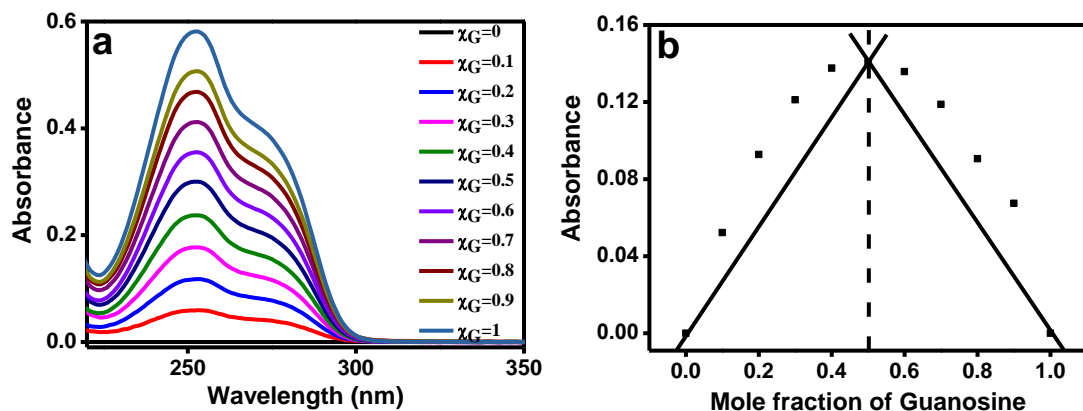


Figure S15. (a) Changes in the UV spectrum of Guanosine (5×10^{-5} M) upon addition of Zinc acetate different molar concentrations and (b) Job's plot obtained by following the absorbance at 251 nm, indicating a 1:1 metal-ligand stoichiometry.

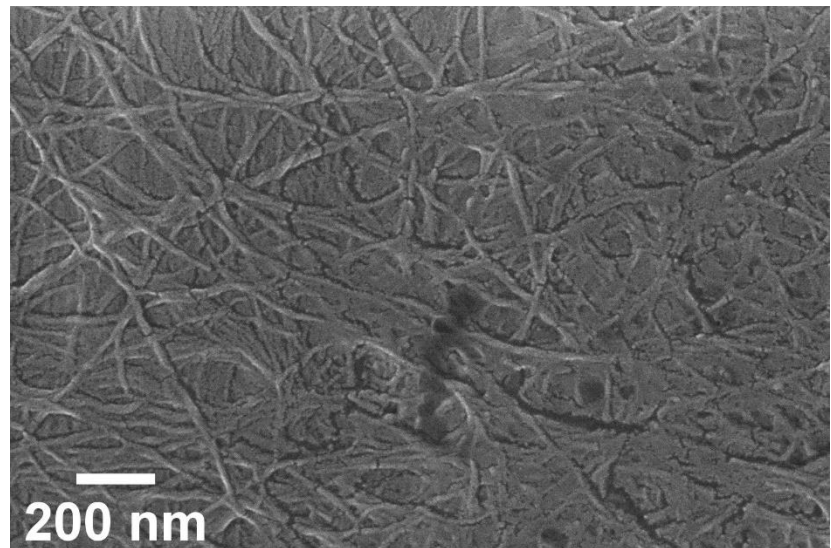


Figure S16. (a) FESEM image of the metallogeal at a concentration of 20 mM for both the precursors showing nanofibrous morphology.

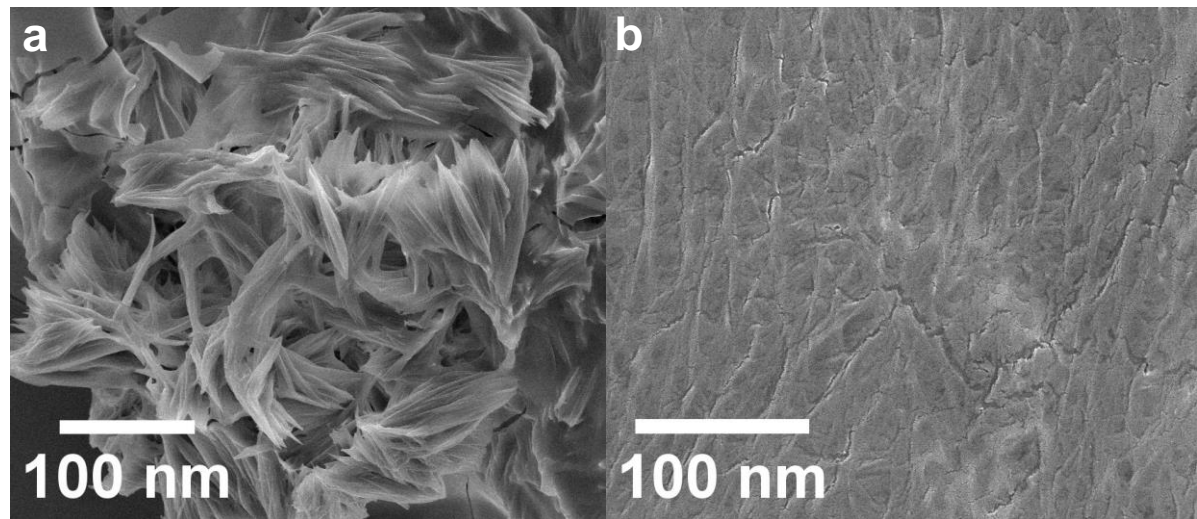


Figure S17. (a) FESEM image of the Zn-guanosine gel at 0 min, and (b) FESEM image of the Zn-guanosine gel just before gelation.

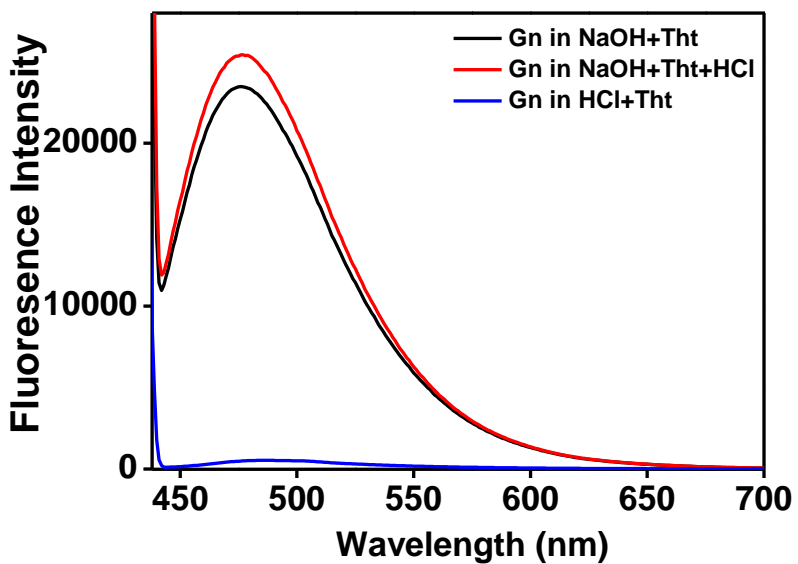


Figure S18. Fluorescence emission spectra of guanosine in NaOH in the presence of Tht (black line), the same guanosine solution in NaOH with Tht after adding HCl (red line) and guanosine in HCl (1M) in the presence of Tht (blue line).

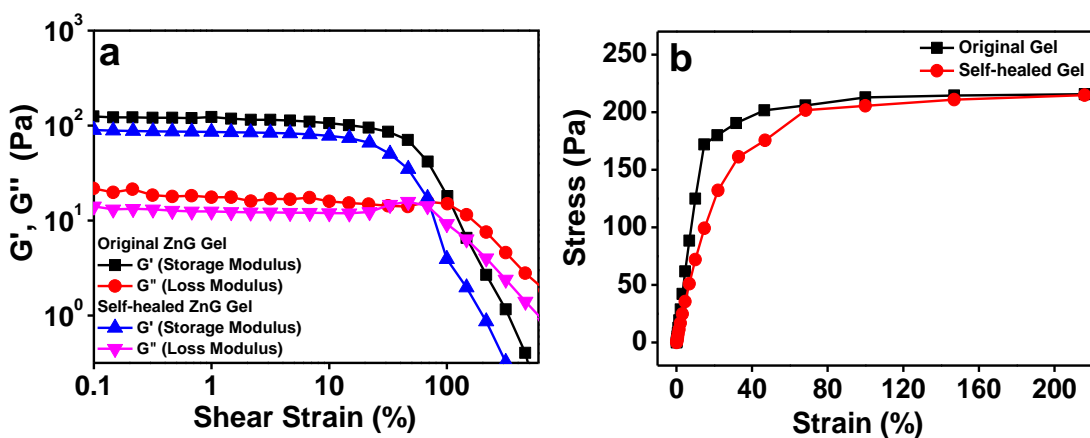


Figure S19. (a) Dynamic strain sweep rheological investigation of the original and self-healed Zn-guanosine gel and (b) Stress-strain curve for representative original and healed samples of Zn-guanosine gel.

Note: It was a plot of strain vs stress rather than a tensile test.

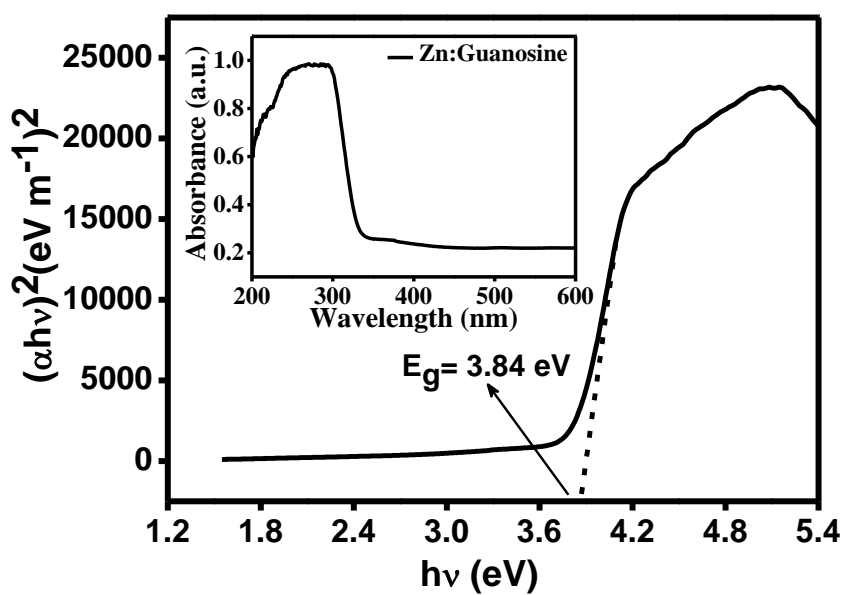
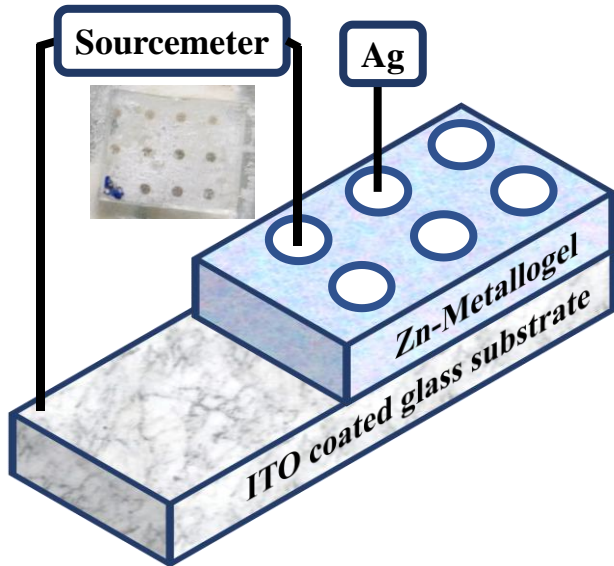


Figure S20. UV–vis absorption spectra (inset) and Tuac’s plots for Zinc-Guanosine metallogel.



Scheme S1. A schematic representation of Schottky diode fabrication using Zn-Guanosine metallogel.

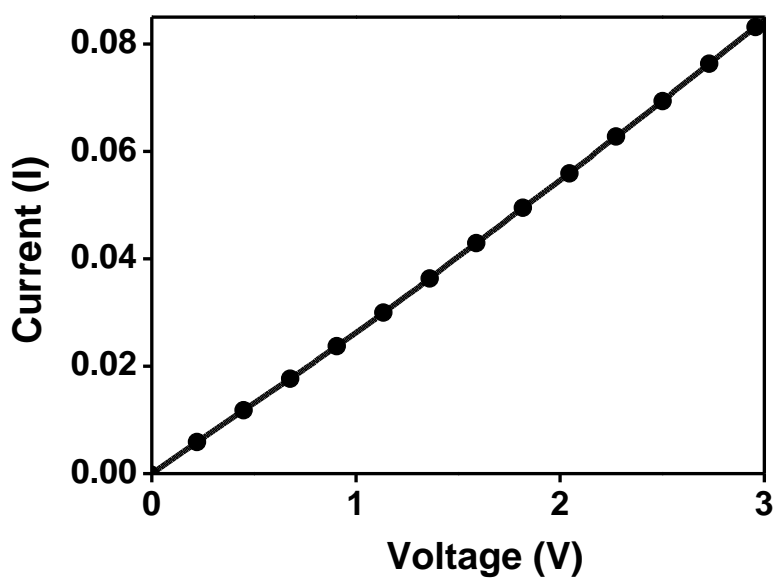


Figure S21. I–V characteristics curve for ITO/Zn-Guanosine Solution (10 mM)/Al structured thin film devices at room temperature.

Table S2. A comparison table including the charge transport parameters of the Zinc-guanosine thin film device.

S.No	Device Name	ON/OFF Ratio	Series Resistance (Ω)	Barrier Height (eV)	Ideality Factor	Reference
1.	Zn-Guanosine	36.5	14.17	0.46	1.99	This Work
2.	Ag/Cu-H₄L	70	65	0.61	3.0	4
3.	Mn@OX	34.65	1092.27	0.22	2.19	5
4.	C₄₀H₃₄Cu₂N₆O₁₈	8.46	81.7	0.47	2.78	6
5.	ZnCdS	29	17300	0.28	2.22	7
6.	Mg@MEA	85.52	725.11	0.38	1.89	8
7.	Zn-AA	49.63	3790	0.45	2.16	9
8.	[Cd₄L₂(NCO)₆]_n	12.44	5306	0.52	3.45	10
9.	Zn@TA	37.06	3751.26	0.47	3.78	11

References:

- 1 L. Martínez, A. Ricardo, E. G. Birgin and J. M. Martínez, *J. Comput. Chem.*, 2009, **30**, 2157–2164.
- 2 W. L. Jorgensen, D. S. Maxwell and J. Tirado-Rives, *J. Am. Chem. Soc.*, 1996, **118**, 1225–11236.
- 3 B. Hess, C. Kutzner, D. Van Der Spoel and E. Lindahl, *J. Chem. Theory Comput.*, 2008, **4**, 435–447.
- 4 V. Kumar, R. K. Upadhyay, D. Bano, S. Chandra, D. Kumar, S. Jit and S. H. Hasan, *New J. Chem.*, 2021, **45**, 6273–6280.
- 5 S. Dhibar, A. Dey, A. Dey, S. Majumdar, D. Ghosh, P. P. Ray and B. Dey, *ACS Appl. Electron. Mater.*, 2019, **9**, 1899–1908.
- 6 A. Hossain, A. Dey, S. K. Seth, P. P. Ray, P. Ballester, R. G. Pritchard, J. Ortega-Castro, A. Frontera and S. Mukhopadhyay, *ACS Omega*, 2018, **3**, 9160–9171.
- 7 M. Das, J. Datta, R. Jana, S. Sil, S. Halder and P. P. Ray, *New J. Chem.*, 2017, **41**, 5476–5486.
- 8 S. Dhibar, A. Dey, A. Dey, S. Majumdar, A. Mandal, P. P. Ray and B. Dey, *New J. Chem.*, 2019, **43**, 15691–15699.
- 9 K. Karmakar, A. Dey, S. Dhibar, R. Sahu, S. Bhattacharjee, P. Karmakar, P. Chatterjee, A. Mondal and B. Saha, *RSC Adv.*, 2023, **13**, 2561–2569.
- 10 P. Ghorai, A. Dey, P. Brandão, J. Ortega-Castro, A. Bauza, A. Frontera, P. P. Ray and A. Saha, *Dalton Trans.*, 2017, **46**, 13531–13543.
- 11 S. Majumdar, A. Dey, R. Sahu, G. Lepcha, A. Dey, P. P. Ray and B. Dey, *Mater. Res. Bull.*, 2023, **157**, 112003.